

## The effect of $f_{O_2}$ on the partitioning and valence of V and Cr in garnet/melt pairs and the relation to terrestrial mantle V and Cr content

K. RIGHTER,<sup>1,\*</sup> S. SUTTON,<sup>2,3</sup> L. DANIELSON,<sup>1</sup> K. PANDO,<sup>1</sup> G. SCHMIDT,<sup>5</sup> H. YANG,<sup>5</sup> S. BERTHET,<sup>4</sup>  
M. NEWVILLE,<sup>2</sup> Y. CHOI,<sup>2</sup> R.T. DOWNS,<sup>5</sup> AND V. MALAVERGNE<sup>4</sup>

<sup>1</sup>NASA Johnson Space Center, Houston, Texas 77058, U.S.A.

<sup>2</sup>GSECARS, 5734 S. Ellis, University of Chicago, Chicago, Illinois 60637, U.S.A.

<sup>3</sup>Department of the Geophysical Sciences, 5734 S. Ellis, University of Chicago, Chicago, Illinois 60637, U.S.A.

<sup>4</sup>Universite Paris Est – Marne La Vallée, Laboratoire des Geomatériaux, Champs-sur-Marne, 77454 Marne La Vallée Cedex, France

<sup>5</sup>Department of Geosciences, University of Arizona, Tucson, Arizona 85721, U.S.A.

### ABSTRACT

Chromium and vanadium are stable in multiple valence states in natural systems, and their distribution between garnet and silicate melt is not well understood. Here, the partitioning and valence state of V and Cr in experimental garnet/melt pairs have been studied at 1.8–3.0 GPa, with variable oxygen fugacity between IW-1.66 and the Ru-RuO<sub>2</sub> (IW+9.36) buffer. In addition, the valence state of V and Cr has been measured in several high-pressure (majoritic garnet up to 20 GPa) experimental garnets, some natural megacrystic garnets from the western United States, and a suite of mantle garnets from South Africa. The results show that Cr remains in trivalent in garnet across a wide range of oxygen fugacities. Vanadium, on the other hand, exhibits variable valence state from 2.5 to 3.7 in the garnets and from 3.0 to 4.0 in the glasses. The valence state of V is always greater in the glass than in the garnet. Moreover, the garnet/melt partition coefficient,  $D(V)$ , is highest when V is trivalent, at the most reduced conditions investigated (IW-1.66 to FMQ). The  $V^{2.5+}$  measured in high  $P$ - $T$  experimental garnets is consistent with the reduced nature of those metal-bearing systems. The low V valence state measured in natural megacrystic garnets is consistent with  $f_{O_2}$  close to the IW buffer, overlapping the range of  $f_{O_2}$  measured independently by Fe<sup>2+</sup>/Fe<sup>3+</sup> techniques on similar samples. However, the valence state of V measured in a suite of mantle garnets from South Africa is constant across a 3 log  $f_{O_2}$  unit range (FMQ-1.8 to FMQ-4.5), suggesting that the valence state of V is controlled by the crystal chemistry of the garnets rather than  $f_{O_2}$  variations. The compatibility of V and Cr in garnets and other deep mantle silicates indicates that the depletion of these elements in the Earth's primitive upper mantle could be due to partitioning into lower mantle phases as well as into metal.

**Keywords:** Garnet, silicate melt, mantle, siderophile

### INTRODUCTION

Garnet is one of the most important host minerals for V and Cr in the upper mantle, where both have a larger concentration than in the bulk silicate Earth (Fig. 1). Furthermore, partition coefficients (or  $D$ , defined as wt% element in phase 1/wt% element in phase 2)  $D(V)$  and  $D(Cr)$  garnet/melt can be as high as six (Trønnes et al. 1992; Canil and Wei 1992), making garnet an important control on trace element partitioning during fractionation in the mantle or a magma ocean. Even though garnet is a known host phase for both V and Cr, almost nothing is known about the valence state of these multi-valent elements (V exhibits 2+, 3+, or 4+, whereas Cr exhibits 2+ or 3+) in garnet (Gunsner et al. 1994; Sitepu et al. 2005). Because V and Cr can have variable valence state (e.g., Schreiber et al. 1987; Berry et al. 2006), it is not clear if the compatibility of V and Cr in garnet is sustained across all natural oxygen fugacities (which varies over 10 log  $f_{O_2}$  units; Righter et al. 2006a), or whether they are compatible in a narrow range that is coincidentally the same as that of the

terrestrial and other planetary mantles.

We have undertaken a study of the valence state of V and Cr in garnet-silicate melt pairs. We carried out a series of experiments on garnet/melt equilibria under a range of  $f_{O_2}$  conditions, from the high- $f_{O_2}$  Ru-RuO<sub>2</sub> buffer to below the Fe-FeO buffer, as well as intermediate values using graphite-CO<sub>2</sub>-CO equilibria and the Mo-MoO<sub>3</sub> buffer. It is expected that there may be a transition from 3+ to 2+ in both V and Cr at lower  $f_{O_2}$  values. Determining whether  $D(V)$  and  $D(Cr)$  increase or decrease amid such a transition is a primary goal. The experimental run products were analyzed using electron microprobe analysis (EMPA), X-ray diffraction (XRD), and micro-X-ray absorption near-edge spectroscopy (XANES). Results are applied to our understanding of V and Cr depletions in mantles, planetary differentiation, and mantle melting.

### EXPERIMENTAL METHODS

Most of the experiments in this study involved equilibration of garnet and silicate melt, but there were also a few garnet synthesis experiments.

Low-pressure experiments were conducted at 1.8 and 3.0 GPa and 1275 °C, for durations of 24 to 48 h and power quenched, in 13 and 10 mm piston-cylinder

\* E-mail: kevin.righter-1@nasa.gov

apparatuses at NASA Johnson Space Center (JSC) (calibrated by Filiberto et al. 2008). Synthetic basalt, seeded with Buell Park, Arizona, megacrystic garnet seeds (see below) was used to stabilize garnet in equilibrium with silicate melt (Table 1 and Fig. 2). To some experiments 1%  $V_2O_5$ , and to some 1%  $Cr_2O_3$  (Table 1) were added. Four different oxygen buffers were imposed on the samples. The highest  $f_{O_2}$  was the Ru-RuO<sub>2</sub> buffer, near the hematite-magnetite buffer (O'Neill and Nell 1997). The second highest  $f_{O_2}$  experiment was carried out at the Mo-MoO<sub>3</sub> buffer (O'Neill 1986), which is about 1 log  $f_{O_2}$  unit above the iron-wüstite buffer (IW). The third highest  $f_{O_2}$  was that of the C-CO-CO<sub>2</sub> (graphite) buffer in a Pt capsule (e.g.,

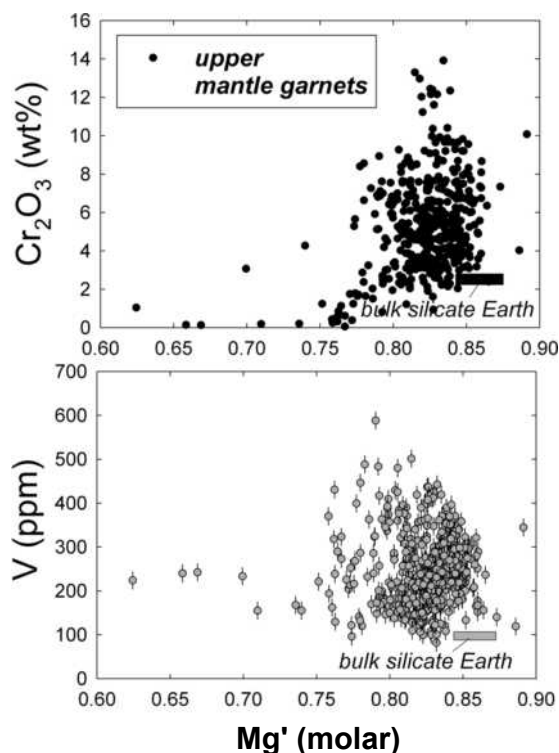


**FIGURE 1.** Vanadium and  $Cr_2O_3$  contents of mantle derived garnets plotted against molar  $Mg'$  [=Mg/(Mg+Fe)] from peridotites, pyroxenites, megacrysts, and xenocrysts in basalt, kimberlite, and lamproite (data from Canil et al. 2003; Roden and Shimizu 2000; Schulze et al. 2006; Scully et al. 2004; Shimizu and Allegre 1978). Errors shown are typical for microprobe analyses of  $Cr_2O_3$  by microprobe (0.1 wt%) and for laser ablation inductively coupled mass spectrometry or secondary ion mass spectrometry for V (20 ppm). Bulk silicate earth (BSE) values are from McDonough and Sun (1995).

**TABLE 1.** Summary of experimental runs

Sample	Pressure (GPa)	$T$ (°C)	Dur.	Buffer	Capsule	Dope	D(V)	D(Cr)	log $f_{O_2}$	IW
VGar5	3.0	1275	6.5 h	Fe-FeO	C	V	8.0	—	-12.26(5)	-1.66(8)
146 (Mo-1)	1.8	1275	24 h	Mo-MoO <sub>3</sub>	Mo	V	3.2	5.3	-9.38(5)	+1.01(8)
216	1.85	1275	11.5 h	CCO	Pt-C	Cr	—	3.6	-9.50(5)	+0.87(8)
224 (Ru-1)	1.85	1275	24 h	Ru-RuO <sub>2</sub>	AuPd	Cr,V	0.40	45	-0.78(5)	+9.59(8)
411	1.85	1275	30 h	Mo-MoO <sub>3</sub>	Mo	Cr	—	15.4	-9.34(5)	+1.03(8)
412	1.85	1275	30 h	CCO	Pt-C	V	2.5	2.2	-9.50(5)	+0.87(8)
413	1.85	1275	30 h	CCO	Pt-C	Cr	—	39.2	-9.50(5)	+0.87(8)
S3567	20	2000	5 min	—	C	V	—	—	—	-2.4(2)
S3568	20	2000	4 min	—	C	V	—	—	—	-2.7(2)
BJJB-43	18.4	1900	10 min	—	C	—	—	—	—	-2.0(2)
BJJB-44	19.4	2000	7 min	—	C	—	—	—	—	-2.0(2)
172	4.0	1575	1.6 h	—	Pt-C	—	—	—	—	—
VGar2	0.8	1200	12 h	—	C	—	—	—	—	—
VGar3	1.0	1300	10 h	—	C	—	—	—	—	—

Notes: Ru-RuO<sub>2</sub> buffer is from O'Neill and Nell (1997); Mo-MoO<sub>3</sub> buffer is from O'Neill (1986); C-O surface is from French and Eugster (1965), and IW reference buffer is from O'Neill (1987). All values calculated at elevated pressures by making a small correction based on the V of reaction, with volumes of metals and oxides taken from Robie et al. (1978).

Frost and Wood 1997; French and Eugster 1965). Finally, the lowest  $f_{O_2}$  experiment was 1.66 log  $f_{O_2}$  units below IW buffer; it was kept reduced by including metallic Si in the starting materials (graphite capsule). This promotes reduced conditions in the capsule (variable Si/O ratio) and results in a small amount of Si alloyed with the Fe and C (e.g., Gessmann et al. 1999; Berthet et al. 2009). In this experiment, the metal contained 93.1% Fe, 0.1 wt% Si, and 4.8 wt% C. The pressure was slightly higher in this experiment (3.0 GPa) to ensure garnet stability in this bulk composition because some FeO is lost to Fe metal in the more reduced experiments. Values for the log  $f_{O_2}$  for the buffers mentioned above were calculated at elevated pressure by making a small correction to the 1 bar value using the expression:  $\log f_{O_2}(P-T) = \log f_{O_2}(T) + C(P-1)/T$  where  $C = -\Delta V/2.303R$  (e.g., Chou 1987), and volume data from Robie et al. (1978). All experiments contained garnet and silicate melt, and a few also contained pyroxene and/or spinel (Fig. 2a).

Several additional experiments were carried out at higher pressures than 1.8 GPa. One experiment was carried out as part of a study of W partitioning between high-pressure minerals and melts (Righter and Shearer 2003). Experiment 172 used a Hawaiian ankaramite at an intermediate pressure of 4.0 GPa, 1575 °C, and equilibrated garnet, clinopyroxene, and melt. Two experiments (BJJB-43 and -44) were conducted in a multi-anvil apparatus at NASA JSC as part of a high  $P$ - $T$  phase equilibrium study of the Richardton H5 ordinary chondrite (Channon et al. 2007). Both contained majoritic garnet and silicate melt and were equilibrated at 18 to 19 GPa and 1900–2000 °C. The highest pressure experiments (S3567 and S3568) were conducted in a multi-anvil apparatus in Bayreuth, Germany (Berthet 2009). These experiments are part of a phase equilibrium study carried out on the Indarch enstatite chondrite (Berthet et al. 2006, 2009), and used 20 GPa and 2000 °C (Table 1). All of these 18–20 GPa experiments were equilibrated between IW-2 and IW-2.6 (Table 1), as calculated using the composition of the metal ( $X_{Fe}$ ) and silicate melt ( $X_{FeO}$ ) in each experiment.

Synthetic goldmanite,  $Ca_3V_2Si_3O_{12}$ , was synthesized at 0.8 and 1.0 GPa, 1200 and 1300 °C, respectively. In addition to the goldmanite, there were also excess  $SiO_2$ ,  $V_2O_5$ , and  $CaSiO_3$ , and quenched liquid (in the 1300 °C experiment; Fig. 2b). These two experiments were carried out in graphite capsules that typically buffer  $f_{O_2}$  near FMQ-2 (Médard et al. 2008; Righter et al. 2009). These samples served as V standards for XANES, and were used to verify the energy and intensity of  $V^{3+}$  in the garnet structure (see later section). Their structure and site occupancy were verified by single-crystal XRD. The previous synthesis experiments of Strens (1965) at 0.3 GPa and 530 °C indicate that goldmanite is stable across a wide  $P$ - $T$  range. This conclusion is also supported by its recovery from low- and high-grade metamorphic rocks (Osanaï et al. 1990; Uher et al. 2008; Moench and Meyrowitz 1964; Pan and Fleet 1992).

## NATURAL SAMPLES

Two natural garnets—uvarovite  $Ca_3Cr_2Si_3O_{12}$  and goldmanite  $Ca_3V_2Si_3O_{12}$ —were also used as standards for the XANES analyses, with single-crystal XRD analysis carried out for structural determination, site occupancy, and stoichiometry. The uvarovite is from the Ural Mountains, Russia, and was provided by the RRUFF project at the University of Arizona (<http://rruff.info/>; sample R060477). The goldmanite is from Tetitice, Klatovy, Czech Republic, and was also provided by the RRUFF project (R061138).

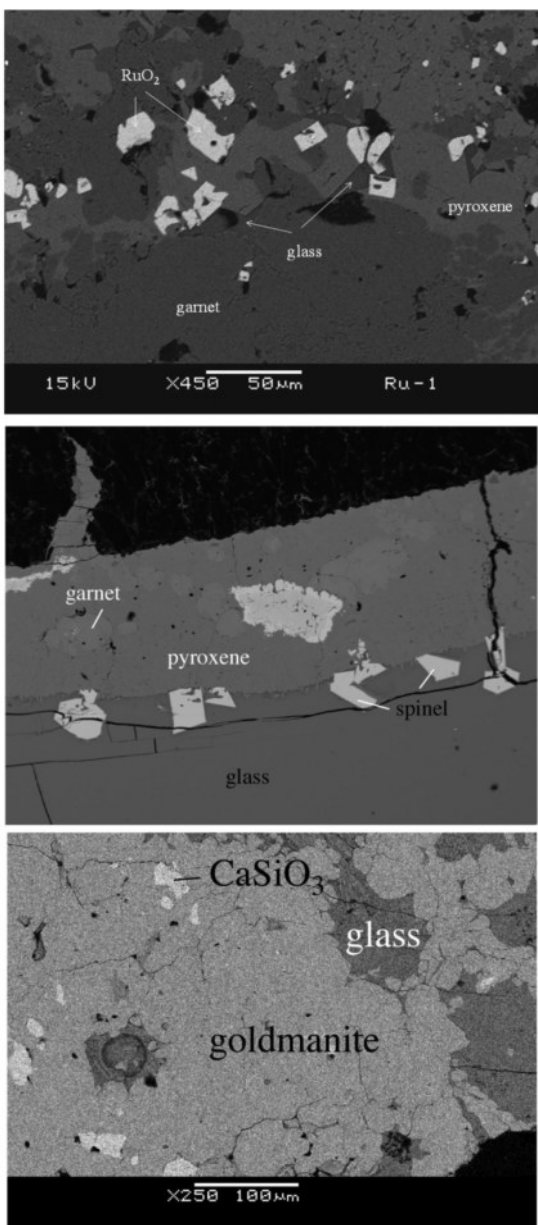


**FIGURE 2. (top)** Backscattered electron image of experiment Ru-1 (224). Garnet, pyroxene, and glass all equilibrated at 1.85 GPa, 1275 °C, and IW+9.59. The high  $f_{O_2}$  was set by the Ru-RuO<sub>2</sub> buffer. **(middle)** Backscattered electron image of experiment no. 412 showing glass, garnet, pyroxene, and bright spinel. Scale bar not shown, but is the same as in the top panel. **(bottom)** Backscattered electron image of run product Vgar-3 showing the dominant phase synthetic goldmanite, and excess CaSiO<sub>3</sub> and silicate glass.

Natural garnets were analyzed to assess valence states of Cr and V in natural samples. These included three megacrystic pyrope crystals from the U.S.A. and Europe: pyrope-rich garnet crystals from a diatreme at Buell Park, Arizona (O'Hara and Mercy 1966; Switzer 1977; Cygan and Lasaga 1985), and from Apache County, Arizona (R060441), and pyrope from Meronitz, Bohemia (R040159). Additionally, five garnets were analyzed from a suite of very well-characterized South African kimberlite xenoliths garnets (from Iherzolites and harzburgites) from the studies

of Woodland and Koch (2003), Lazarov et al. (2009), and Peslier et al. (2008). The samples selected from these studies are from the Kimberley, Lesotho, Jagersfontein, and Finsch localities and cover a large range of  $f_{O_2}$  from FMQ-1.8 to FMQ-4.5 (Liq-11 = FMQ-3.45, Jag-1 = FMQ-4.4, Jag-4 = FMQ-3.21, KIM-24 = FMQ-1.81, and 554-XM46 = FMQ-4.54; Woodland and Koch 2003; Lazarov et al. 2009; Peslier et al. 2008) and, thus, may show some evidence for variable valence state if present.

## ANALYTICAL METHODS

### Electron microprobe analysis (EMPA)

All major elements in garnets, pyroxenes, spinels, and glasses were analyzed with a CAMECA SX100 electron microprobe (at NASA-JSC), using an accelerating voltage of 20 kV and sample current of 20 nA. Standards included both natural (kaersutite, andradite, wollastonite, chromite, rutile, olivine, rhodonite, potassium feldspar, albite) and synthetic (V metal, NiO) standard materials. Count times for major elements were typically 10 s, and as long as 120 s for low concentrations of V or Cr in garnets and glasses. Under the latter conditions, detection limits were approximately 100 ppm for V. Interference of TiK $\alpha$  on VK $\alpha$  peaks (Snetsinger et al. 1968) were avoided by counting Ti on PET using integral mode, and V on LiF in differential mode. PAP  $\phi$ - $\rho$ -Z corrections were used in the data reduction (Pouchou and Pichoir 1991). All analyses are reported in Tables 2 and 3.

### X-ray absorption near-edge structure (XANES)

X-ray absorption near-edge structure (XANES) spectroscopy is an element-specific technique that can differentiate between oxidation states. K-edge XANES spectra derive from the excitation of a 1s electron to higher energy bound or delocalized (continuum) excited states. Features comprising the pre-edge and edge can be attributed simplistically to transitions between bound electronic states (e.g., 1s  $\rightarrow$  3d, 1s  $\rightarrow$  4s) due to the similarity of the energy differences to those of the (Z + 1) free ion levels

**TABLE 2.** Experimental garnet and glass analyses (1 $\sigma$  in parentheses, applied to last digit or digits of value)

Sample	VGar5	Mo-1	216	Ru-1	411	412	413
<b>Garnet</b>							
SiO <sub>2</sub>	51.5(7)	39.4(5)	38.4(4)	40.7(5)	40.0(4)	38.5(4)	39.6(5)
TiO <sub>2</sub>	1.24(2)	0.04(1)	0.03(1)	0.07(2)	0.06(2)	0.02(1)	0.12(2)
Al <sub>2</sub> O <sub>3</sub>	6.3(2)	19.6(5)	21.7(4)	21.7(4)	21.5(3)	18.5(3)	18.8(4)
Cr <sub>2</sub> O <sub>3</sub>	–	0.21(2)	0.62(3)	0.45(3)	2.00(2)	0.11(1)	5.88(8)
V <sub>2</sub> O <sub>3</sub>	1.63(3)	2.90(5)	0.011(2)	0.079(6)	0.01(1)	4.08(5)	0.03(1)
FeO	14.98(6)	19.96(7)	18.82(8)	8.47(7)	18.05(8)	21.10(8)	16.57(7)
MnO	0.46(3)	0.06(1)	0.10(1)	0.22(2)	0.14(1)	0.03(1)	0.18(2)
MgO	7.4(3)	9.6(3)	10.9(4)	18.3(5)	11.7(2)	7.6(2)	11.5(3)
CaO	14.05(3)	8.17(2)	7.58(2)	7.88(2)	7.16(2)	9.60(3)	8.12(2)
Na <sub>2</sub> O	2.21(11)	–	–	–	–	–	–
Mg'	0.52	0.46	0.51	0.79	0.54	0.39	0.55
Total	99.77	99.89	98.12	97.90	100.66	99.48	100.71
<b>Glass</b>							
SiO <sub>2</sub>	60.5(7)	51.0(6)	51.5(7)	50.9(8)	56.4(7)	50.6(8)	57.0(9)
TiO <sub>2</sub>	1.76(2)	0.08(1)	0.03(1)	0.088(2)	0.17(2)	0.01(1)	0.21(2)
Al <sub>2</sub> O <sub>3</sub>	11.0(3)	13.3(3)	13.8(3)	14.8(3)	15.0(3)	13.1(3)	14.9(3)
Cr <sub>2</sub> O <sub>3</sub>	–	0.04(2)	0.17(2)	0.01(1)	0.13(2)	0.05(1)	0.15(2)
V <sub>2</sub> O <sub>3</sub>	0.20(2)	0.92(4)	0.013(2)	0.20(2)	0.01(1)	1.66(5)	0.01(1)
FeO	12.81(5)	13.69(4)	12.69(4)	8.34(3)	8.51(3)	13.55(5)	8.16(3)
MnO	0.31(2)	0.03(1)	0.03(1)	0.11(1)	0.04(1)	0.01(1)	0.04(1)
MgO	1.3(1)	4.8(2)	4.7(2)	5.8(2)	4.3(2)	4.8(2)	4.0(2)
CaO	5.44(3)	9.88(4)	10.61(3)	10.48(3)	8.95(3)	9.54(3)	8.95(3)
Na <sub>2</sub> O	3.06(9)	–	–	–	–	–	–
Mg'	0.25	0.38	0.40	0.56	0.47	0.39	0.47

**TABLE 3.** Natural and experimental garnets (1 $\sigma$  in parentheses, applied to last digit or digits of value)\*

Sample	Uvarovite R060477	Goldmanite R061138	Bohemia R040159	Buell Mtn	Apache R060441	Liq-11	Jag-1	Jag-4	Kim-24	554-XM46
<b>Natural</b>										
SiO <sub>2</sub>	36.30(58)	36.28(14)	43.08(22)	40.8(4)	41.44(21)	41.3	42.3	42.6	42.0	40.9
TiO <sub>2</sub>	1.31(6)	1.18(21)	0.52(1)	0.07(1)	–	0.03	0.32	0.57	–	0.11
Al <sub>2</sub> O <sub>3</sub>	8.52(50)	2.20(34)	21.51(14)	23.0(4)	22.70(11)	20.2	18.9	21.4	20.0	17.7
Cr <sub>2</sub> O <sub>3</sub>	17.12(64)	1.00(23)	1.96(4)	0.94(3)	0.79(2)	4.57	5.25	1.67	5.35	7.4
V <sub>2</sub> O <sub>3</sub>	–	24.41(43)	–	0.02(1)	–	–	–	–	–	–
FeO	0.20(3)	1.07(12)	8.16(14)	7.22(4)	12.61(12)	6.4	6.98	7.94	6.46	6.79
MnO	–	1.79(12)	0.25(3)	0.34(2)	0.45(4)	0.31	0.23	0.27	0.30	0.36
MgO	–	0.20(2)	20.51(18)	20.0(5)	16.93(13)	21.2	21.4	21.9	21.6	19.8
CaO	34.65(19)	31.44(14)	4.50(4)	5.57(3)	4.99(6)	5.38	5.07	4.26	5.19	6.21
Na <sub>2</sub> O	0.02(1)	–	–	–	–	0.02	0.04	0.08	0.04	0.02
Mg <sup>i</sup>	0.00	0.25	0.82	0.83	0.71	0.86	0.85	0.83	0.86	0.84
Total	98.16	99.68	100.53	97.97	99.91	99.69	100.45	100.72	100.98	99.29
Sample	172	S3567	S3568	BJJB-43	BJJB-44	VGar2	VGar3			
<b>Experimental</b>										
SiO <sub>2</sub>	40.0(5)	53.0(6)	55.9(8)	50.6(6)	52.2(7)	34.9(5)	34.9(5)			
TiO <sub>2</sub>	1.48(2)	–	–	0.08(2)	0.03(1)	–	–			
Al <sub>2</sub> O <sub>3</sub>	21.2(5)	4.6(2)	3.5(2)	4.6(2)	9.2(3)	–	–			
Cr <sub>2</sub> O <sub>3</sub>	–	0.89(3)	0.74(3)	0.86(3)	1.30(5)	–	–			
V <sub>2</sub> O <sub>3</sub>	–	–	–	–	–	30.84(3)	31.15(3)			
FeO	12.49(3)	5.75(2)	4.60(3)	9.50(4)	4.84(3)	–	–			
MnO	0.27(2)	0.28(2)	0.32(2)	0.33(2)	0.24(2)	–	–			
MgO	15.2(3)	31.0(4)	31.6(4)	31.4(4)	30.3(4)	–	–			
CaO	9.39(3)	1.03(3)	1.12(3)	1.82(3)	1.00(3)	33.60(8)	33.93(7)			
Na <sub>2</sub> O	–	–	–	0.62(4)	0.27(2)	–	–			
Mg <sup>i</sup>	0.68	0.91	0.92	0.85	0.92	–	–			
Total	101.96	97.30	98.64	99.90	99.36	99.32	100.01			

\* Microprobe data for samples from the RRUFF project (R number in table) are from the RRUFF database (<http://rruff.info/>); analyses of samples Liq-11, Jag-1, Jag-4, Kim-24, 554-XM46 are from Woodland and Koch (2003) and Lazarov et al. (2009).

(Shulman et al. 1976; Waychunas et al. 1983). The edge and its component transitions may vary in both energy and intensity with oxidation state. Transitions shift to higher energies with increasing charge ( $\sim 1$  eV/charge) and this trend can be used for quantifying oxidation state ratios (Wong et al. 1984; Sutton et al. 1993; Bajt et al. 1994; Berry et al. 2003).

In the case of V, the energy and intensity of the pre-edge peak has been shown to be a systematic function of  $f_{O_2}$ , and the work of Sutton et al. (2005) on glasses and Righter et al. (2006b) on spinels serves as a foundation for the extension to garnets. The oxidation state of V was inferred from the normalized intensity of the pre-edge peak. For details of the V XANES analyses, readers are referred to the work of Sutton et al. (2005) and Righter et al. (2006b).

In the case of Cr, the  $1s \rightarrow 3d$ ,  $1s \rightarrow 4s$ , main edge, and edge crest all systematically vary with oxidation state (Sutton et al. 1993). The intensity of a transition is strongly dependent upon the coordination environment because transitions such as  $1s \rightarrow 3d$  and  $1s \rightarrow 4s$  are symmetry forbidden but may gain intensity from orbital mixing in low-symmetry environments (Shulman et al. 1976). A shoulder on the main absorption edge, assigned as the  $1s \rightarrow 4s$  transition (Sutton et al. 1993), systematically changes intensity with  $f_{O_2}$  and must relate quantitatively to the oxidation state of Cr. Studies by Berry and O'Neill (2004) show the expected shift of the main absorption edge to higher energies with increasing oxidation state. Due to the coordination freedom available in a melt, Cr can adopt the coordination geometry for each oxidation state that produces the greatest electronic stabilization. The high-symmetry octahedral geometry favored by Cr<sup>3+</sup> ( $d^3$ ) results in the  $1s \rightarrow 4s$  feature being weak or absent, whereas the transition is allowed for Cr<sup>2+</sup> ( $d^4$ ) due to a Jahn-Teller distortion of the coordination environment. The absorption

edge shoulder may therefore be diagnostic of Cr<sup>2+</sup> in silicates, which suggests that its intensity may be used to quantify Cr<sup>2+</sup>/ $\Sigma$ Cr (Sutton et al. 1993).

The intensity of the  $1s \rightarrow 4s$  transition is most easily quantified from the derivative spectrum in which the shoulder appears as a peak. The area of this peak (from 5991.3 to 5996.3 eV) is linearly correlated with Cr<sup>2+</sup>/ $\Sigma$ Cr (Berry and O'Neill 2004). Energy was calibrated by defining the first derivative peak of Cr in stainless steel foil as 5989.2 eV. Spectra were recorded from 5985–6015 eV using a 0.25 eV step size for a preset fixed time. Typical count times per point were around 5 s for a total scan time of 15–20 min. The oxidation state of Cr was inferred from the intensity of the 5994 eV peak in the derivative spectrum.

A monochromatic X-ray beam ( $3 \times 3 \mu\text{m}$ ) from a Si(111) double-crystal monochromator was focused onto the sample and the fluorescent X-ray yield was plotted as a function of incident X-ray energy (more detail can be found in Sutton et al. 2002). Vanadium-bearing glasses, oxides, and garnets, and Cr<sup>2+</sup> and Cr<sup>3+</sup> glasses were used as standards (Tables 4 and 5). Because garnet is a cubic phase, there should be no orientation effects (similar to what was found in spinels by Righter et al. 2006b). Figure 3 shows that there is no difference between six different measurements of Bohemia garnet grains with random orientation. The determination of valence state was made using previous calibrations of Righter et al. (2006b) for V (Fig. 4), in which the synthetic goldmanite was utilized as a trivalent standard along the oxide/glass calibration. Chromium-bearing standard glasses (Hanson and Jones 1998) were used for determination of Cr<sup>2+</sup> and Cr<sup>3+</sup> in glasses and garnets (Fig. 5). Glass 224 was measured both at Brookhaven and APS and the calculated valence state for V is 4.17 (BNL in 2/09) and 4.33 (APS in 2/07). These values overlap at the  $2\sigma$  level, indicat-

**TABLE 4.** XANES data for V (1 $\sigma$  in parentheses, based on calibration of Sutton et al. 2005)

Sample	Pre-edge peak int. V glass	Energy V glass	Valence V glass	Pre-edge peak int. V garnet	Energy V garnet	Valence V garnet
<b>Natural garnets</b>						
Bohemia	–	–	–	30(3)	–	2.50(0.15)
Buell	–	–	–	33(3)	–	2.52(0.15)
Apache	–	–	–	34(3)	–	2.52(0.15)
Goldmanite	–	–	–	–	–	2.61(0.15), 2.56(0.15), 2.67(0.15), 2.62(0.15), 2.56(0.15)
Liq-11	–	–	–	30(3)	–	2.49(0.15)
Jag-1	–	–	–	36(3)	–	2.55(0.15)
Jag-4	–	–	–	34(3)	–	2.53(0.15)
Kim-24	–	–	–	28(3)	–	2.46(0.15)
554	–	–	–	30(3)	–	2.49(0.15)
<b>Experimental garnets</b>						
Ru-1 (224)	538(60)	–	4.33(0.15) (APS) 4.17(0.15) (BNL)	267(30)	–	3.71 (0.15) (APS)
412	–	–	3.14(0.15)	–	–	garnet: 2.70(0.15), 2.64(0.15); spinel: 2.84(0.15), 2.86 (0.15)
Mo-1	130(12)	–	3.20(0.15)	74(8), 84(8)	–	2.87(0.15), 2.94(0.15)
182	169(17)	–	3.37(0.15)	51(5), 52 (5)	–	2.70(0.15), 2.70(0.15)
216	–	–	–	74(8)	–	2.87(0.15)
S3567	–	–	–	46(4), 49(5)	–	2.65(0.15), 2.68(0.15)
S3568	–	–	–	37(4)	–	2.56(0.15)
BJJB-43	–	–	–	52(5)	–	2.70(0.15)
BJJB-44	–	–	–	50(5)	–	2.70(0.15)

**TABLE 5.** XANES data for Cr (1 $\sigma$  in parentheses, based on calibration of Karner et al. 2007)

Sample	Cr glass (height above deriv. after 7 smooth)	Valence Cr glass	Cr garnet (height above deriv. after 7 smooth)	Valence Cr garnet
<b>Natural garnets</b>				
Bohemia	–	–	0.000–0.005	3.09(0.08)
Buell	–	–	0.001, 0.002	3.11(0.08)
Apache	–	–	0.002	3.09(0.08)
Liq-11 (3)	–	–	–	2.99(0.08)
Jag-1 (3)	–	–	–	3.00(0.08)
Jag-4 (3)	–	–	–	2.99(0.08)
<b>Experimental garnets</b>				
Ru-1 (224)	0.002	3.09(0.08)	0.002	3.09(0.08)
411	–	3.01(0.08)	–	2.99(0.08), pyroxene: 3.00(0.08)
413	–	3.02 (0.08)	–	3.00 (0.08), pyroxene: 3.01(0.08)
Mo-1	–	–	0.001–0.004	3.03(0.08) 3.13(0.08)
216	0.002	3.09(0.08)	0.001	3.13(0.08)
214	0.002	3.09(0.08)	–	–
S3567	–	–	0.001	3.13(0.08)
S3568	–	–	0.002	3.09(0.08)
BJJB	–	–	0.002	3.09(0.08)
172	–	–	0.001	3.13(0.08)

ing that there are no significant differences between sessions at the two beamlines.

### X-ray diffraction (XRD)

Single-crystal structures of four garnet samples were determined by XRD, at the University of Arizona, with the aim of characterizing site occupancy and verifying the valence states of vanadium. Selected crystals included two natural garnets (uvarovite and goldmanite) and the two experimental garnets (VGar2 and VGar3). Data collection was performed with a Bruker X8 single-crystal X-ray diffractometer (MoK $\alpha$  radiation, graphite monochromator) equipped with a CCD area detector. Structural refinements were carried out with SHELXL-97 (Sheldrick 2008). Details are included in Tables 6 and 7. (CIF<sup>1</sup> is also available on deposit.)

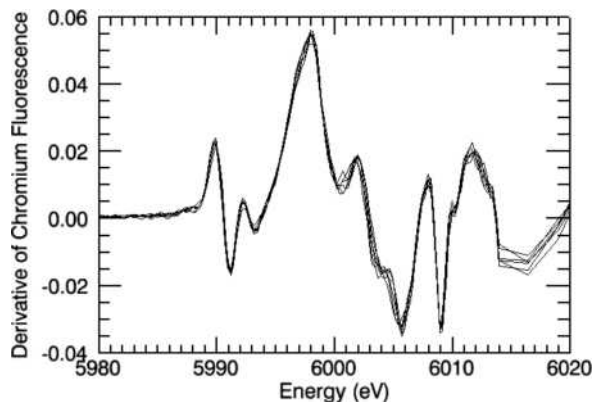


**FIGURE 3.** XANES spectra for six different grains of Bohemia garnet illustrating that the crystal orientation does not have a control on the XANES spectra features, as expected for a cubic garnet structure, and also measured for spinel by Righter et al. (2006b). Spectral features are plotted as the derivative of Cr fluorescence.

## RESULTS

### Garnet XRD results

The structures of the two synthetic garnets are in good agreement with predicted structures for an end-member Ca<sub>3</sub>V<sub>2</sub><sup>3+</sup>Si<sub>3</sub>O<sub>12</sub> garnet (Novak and Gibbs 1971). Unit-cell edges calculated from mean octahedral and dodecahedral cation radii estimated using the microprobe data and the cation radii of Shannon (1976) are 12.07 Å, compared to 12.079 and 12.089 Å derived from the refinement. Similarly, the oxygen positional parameters predicted by Novak and Gibbs (1971) are  $x = 0.0396$ ,  $y = 0.0489$ , and  $z = 0.6547$ , compared to the values of  $x = 0.0392$ – $0.0393$ ,  $y = 0.0476$ – $0.0481$ ,

<sup>1</sup> Deposit item AM-11-045, CIF. Deposit items are available two ways: For a paper copy contact the Business Office of the Mineralogical Society of America (see inside front cover of recent issue) for price information. For an electronic copy visit the MSA web site at <http://www.minsocam.org>, go to the *American Mineralogist* Contents, find the table of contents for the specific volume/issue wanted, and then click on the deposit link there.

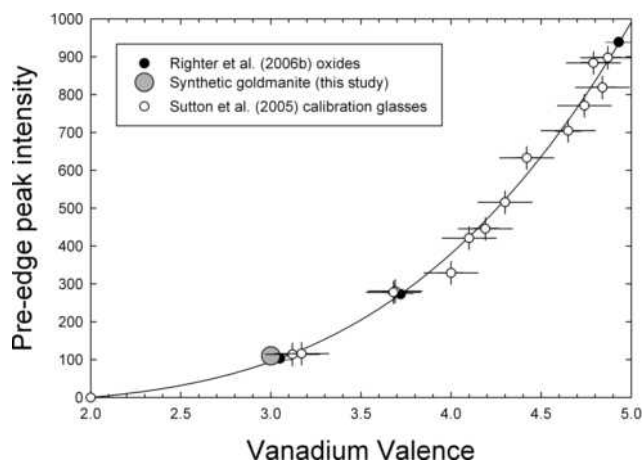


**FIGURE 4.** Valence state of V in silicate melts correlated with pre-edge peak intensity for a series of glasses (Sutton et al. 2005), V-bearing spinel and cavansite (from Righter et al. 2006b), and the synthetic goldmanite  $\text{Ca}_3\text{V}_2\text{Si}_3\text{O}_{12}$  from this study. The correlation of all these isotropic phases indicates that the correlation can be extended to garnets. Error on valence state is  $1\sigma$  error from the calibration of Sutton et al. (2005); error on normalized intensities is also from Sutton et al. (2005) and based on repeated measurements.

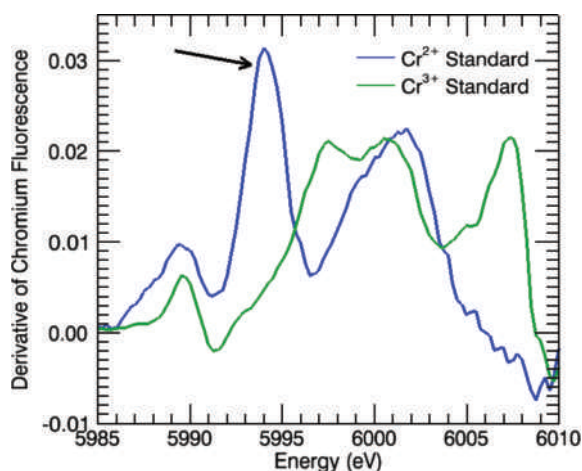


**FIGURE 5.** Derivative of the normalized energy across the Cr  $K$ -edge showing the distinctive  $\text{Cr}^{2+}$  peak at 5994 eV for the  $\text{Cr}^{2+}$  glass standard (arrow). There is no corresponding peak in the  $\text{Cr}^{3+}$  glass standard. (Color online.)

and  $z = 0.6549$ – $0.6551$  derived by refinement analysis.

The natural uvarovite contains Ca, Cr, Al, Ti, V, and Fe, and the formula is  $[\text{Ca}_{2.989}\text{Fe}_{0.011}][\text{Cr}_{1.100}\text{Al}_{0.869}\text{V}_{0.005}\text{Ti}_{0.026}]\text{Si}_3\text{O}_{12}$ . Its structure is also in good agreement with the expected structure of a garnet with this composition (Novak and Gibbs 1971). The unit-cell edge calculated using the mean octahedral and dodecahedral cation radii estimated from the microprobe data and the cation radii of Shannon (1976) is  $11.939 \text{ \AA}$ , slightly larger than the value of  $11.920 \text{ \AA}$  derived from the refinement. Similarly, the oxygen positional parameters predicted by the equations in Novak and Gibbs (1971) are  $x = 0.0387$ ,  $y = 0.0466$ , and  $z = 0.6525$ , and are in excellent agreement with the values of  $x = 0.0388$ ,  $y = 0.0466$ , and  $z = 0.6526$  derived by the experimental refinement analysis.

The natural goldmanite contains Ca, V, Al, Mn, Cr, Fe,

**TABLE 6.** Structural refinement data for four garnets

Parameter	VGar2 (R090043)	VGar3 (R090044)	Uvarovite (R060477)	Goldmanite-nat (R061138)
$a$ ( $\text{\AA}$ )	12.0790(8)	12.0854(12)	11.9204(8)	12.0279(9)
$V$ ( $\text{\AA}^3$ )	1762.35	1765.16	1693.84	1740.08
Space group	$la\bar{3}d$	$la\bar{3}d$	$la\bar{3}d$	$la\bar{3}d$
$2\theta$ range	8.26–69.78	8.26–69.74	9.63–68.67	9.62–69.90
Total reflections	2652	2516	2921	2711
Unique reflections	331	330	298	320
Unique refl. $>2\sigma(I)$	213	150	192	248
$R_{\text{int}}$	0.0386	0.0798	0.0523	0.0273
$R_1$	0.0261	0.0269	0.0284	0.0209
$wR_2$	0.0487	0.0498	0.0722	0.0455
Goodness of fit	1.131	0.966	1.056	1.075
$x$ (calc*)	0.0396	0.0396	0.0387	0.0392
$y$ (calc*)	0.0489	0.0489	0.0466	0.0489
$z$ (calc*)	0.6547	0.6547	0.6525	0.6545
$a$ (calc*) $\text{\AA}$	12.07	12.07	11.939	12.017
$x$	0.0393	0.0392	0.0388	0.0391
$y$	0.0481	0.0476	0.0466	0.0480
$z$	0.6551	0.6549	0.65260	0.6548

\*  $x$ ,  $y$ ,  $z$ , and  $a$  values calculated using the predictive expression of Novak and Gibbs (1971) using the cation radii of Shannon (1976).

Mn, Ti, and Mg, and the formula is  $[\text{Ca}_{2.783}\text{Fe}_{0.074}\text{Mn}_{0.119}\text{Mg}_{0.025}][\text{V}_{1.643}\text{Al}_{0.216}\text{Cr}_{0.066}\text{Ti}_{0.074}]\text{Si}_3\text{O}_{12}$ . On the one hand, its structure is in reasonable agreement with the structure expected for a garnet of this composition and valence state of  $\text{V}^{3+}$  (Novak and Gibbs 1971). The unit-cell edge calculated using the mean octahedral and dodecahedral cation radii estimated from the microprobe data and the cation radii of Shannon (1976) is  $12.006 \text{ \AA}$ , compared to  $12.028 \text{ \AA}$  derived from the refinement. Similarly, the oxygen positional parameters predicted by Novak and Gibbs (1971) are  $x = 0.0391$ ,  $y = 0.0489$ , and  $z = 0.6543$ , compared to the values of  $x = 0.0391$ ,  $y = 0.0480$ , and  $z = 0.6549$  derived by refinement analysis. If, on the other hand, we assume that the V is distributed as  $\text{V}_{1.569}^{3+}\text{V}_{0.074}^{2+}$ , such that the chemical formula exhibits charge balance, then the calculated parameters are  $a = 12.017 \text{ \AA}$ ,  $x = 0.0392$ ,  $y = 0.0489$  and  $z = 0.6545$ , and these parameters match those observed significantly better than those computed with only trivalent V state. Because the substitution of  $\text{V}^{2+}$  for  $\text{V}^{3+}$  increases the size of the unit cell, we computed the distribution that best reproduces the unit-cell parameter as  $\text{V}_{1.492}^{3+}\text{V}_{0.151}^{2+}$ ; in other words, the best fit occurs when 9% of the V is in the  $\text{V}^{2+}$  state.

## Vanadium XANES

For the valence state discussions here and below, we will characterize a mixture of cations with differing valence states to one significant figure; for example a valence state of 2.5 indicates 50% 2+ and 50% 3+, or the average of the two. In the series of samples at variable  $f_{\text{O}_2}$  at 1.8 GPa, average V valence state in garnet varies from  $<3+$  at low  $f_{\text{O}_2}$  ( $\Delta\text{IW} = +0.87$ ) to  $>3+$  at high  $f_{\text{O}_2}$  ( $\Delta\text{IW} = +9.59$ ; Fig. 6a). In addition, glass coexisting with garnet has a V valence state that is always higher than the garnet (Figs. 6a and 7), with the exception of lowest  $f_{\text{O}_2}$  of  $\Delta\text{IW} = +0.87$ . The most reduced experiment shows that the silicate melt and garnet have nearly the same valence state at  $f_{\text{O}_2}$  of  $\Delta\text{IW} = +0.87$ . The higher  $f_{\text{O}_2}$  results show higher V valence state in glasses, but the valence states of both converges at low  $f_{\text{O}_2}$ . If the silicate melt continues to reduce V at  $< \text{IW}-2$ , and the valence state in the garnet continues to stay at 2.5, it is possible that at very low  $f_{\text{O}_2}$  (IW-3), V valence state becomes lower in the glass

**TABLE 7.** Atomic coordinates and displacement parameters for four garnets

	Atom	x	y	z	Occ	$U_{10}$	$U_{11}$	$U_{22}$	$U_{33}$	$U_{12}$	$U_{13}$	$U_{23}$
VGar2	Ca	0.125	0	0.25		0.0074(3)	0.0061(4)	0.0080(3)	0.0080(3)	0	0	0.0014(3)
	V	0	0	0		0.0053(2)	0.0053(2)	0.0053(2)	0.0053(2)	0.0002(2)	0.0002(2)	0.0002(2)
	Si	0.375	0	0.25		0.0052(3)	0.0045(5)	0.0055(3)	0.0055(3)	0	0	0
	O	0.0393(1)	0.0482(1)	0.6553(1)		0.0092(4)	0.0091(6)	0.0088(7)	0.0097(7)	0.0004(5)	-0.005(5)	-0.0002(5)
VGar3	Ca	0.125	0	0.25		0.0078(3)	0.0056(6)	0.0088(4)	0.0088(4)	0	0	0.0088(4)
	V	0	0	0		0.0057(3)	0.0057(3)	0.0057(3)	0.0057(3)	0.0006(3)	0.0006(3)	0.0006(3)
	Si	0.375	0	0.25		0.0054(4)	0.0042(7)	0.0060(5)	0.0060(5)	0	0	0
	O	0.0393(2)	0.0477(2)	0.6550(2)		0.0118(5)	0.014(1)	0.010(1)	0.010(1)	-0.0003(7)	-0.0014(8)	0.0002(8)
Uvarovite	Ca	0.125	0	0.25		0.0026(3)	0.0014(4)	0.0032(4)	0.0032(4)	0	0	0.0007(3)
	Cr	0	0	0	0.575(1)	0.0067(4)	0.0067(4)	0.0067(4)	0.0067(4)	0.0001(2)	0.0001(2)	0.0001(2)
	Al	0	0	0	0.410(1)	0.0067(4)	0.0067(4)	0.0067(4)	0.0067(4)	0.0001(2)	0.0001(2)	0.0001(2)
	Ti	0	0	0	0.015(1)	0.0067(4)	0.0067(4)	0.0067(4)	0.0067(4)	0.0001(2)	0.0001(2)	0.0001(2)
	Si	0.375	0	0.25		0.0032(5)	0.0036(7)	0.0031(5)	0.0031(5)	0	0	0
	O	0.0388(1)	0.0466(1)	0.6526(1)		0.0094(4)	0.0106(7)	0.0097(8)	0.0079(7)	0.0004(5)	-0.0005(5)	0.0003(5)
Goldmanite-nat	Ca	0.125	0	0.25	0.927(1)	0.0075(2)	0.0055(2)	0.0086(2)	0.0086(2)	0	0	0.0014(1)
	Mn	0.125	0	0.25	0.057(1)	0.0075(2)	0.0055(2)	0.0086(2)	0.0086(2)	0	0	0.0014(1)
	V	0	0	0	0.810(1)	0.0050(2)	0.0050(2)	0.0050(2)	0.0050(2)	0.00007(8)	0.00007(8)	0.00007(8)
	Al	0	0	0	0.110(1)	0.0050(2)	0.0050(2)	0.0050(2)	0.0050(2)	0.00007(8)	0.00007(8)	0.00007(8)
	Cr	0	0	0	0.080(1)	0.0050(2)	0.0050(2)	0.0050(2)	0.0050(2)	0.00007(8)	0.00007(8)	0.00007(8)
	Si	0.375	0	0.25		0.0040(2)	0.0045(3)	0.0037(3)	0.0037(3)	0	0	0
	O	0.03916(8)	0.04789(8)	0.65493(8)		0.0082(2)	0.0084(4)	0.0083(4)	0.0079(4)	0.0002(3)	-0.0001(3)	0.0003(3)

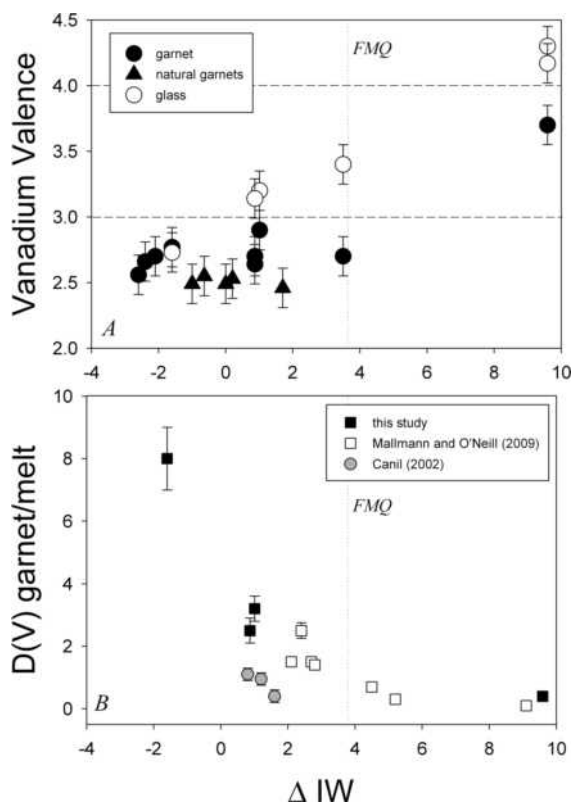


**FIGURE 6.** (a) Summary of V valence state in some natural garnets, and garnet-glass pairs across a range of  $f_{O_2}$  in this study. Natural garnet V valence state, with  $f_{O_2}$  calculated according to the studies of Woodland and Koch (2003) and McCammon and Lazarov (2004), show no trend with  $f_{O_2}$ , and a value close to 2.5. For experimental samples, V valence state in garnet varies from +2.6 at low  $f_{O_2}$  to +3.7 at high  $f_{O_2}$ , whereas glass V valence state is always higher than the coexisting garnet. Error on valence state is  $1\sigma$  error from the calibration of Sutton et al. (2005); vertical dashed line is the value of the FMQ buffer for comparison. (b) Variation in  $D(V)$  garnet/melt with valence state and  $f_{O_2}$ . Data of Mallmann and O'Neill (2009) and Canil (2002) for a smaller  $f_{O_2}$  range showing consistency with our data at the same range. For both diagrams (a and b), oxygen fugacity is relative to the IW buffer ( $\Delta IW$ ), calculated at the temperature of the individual experiments.

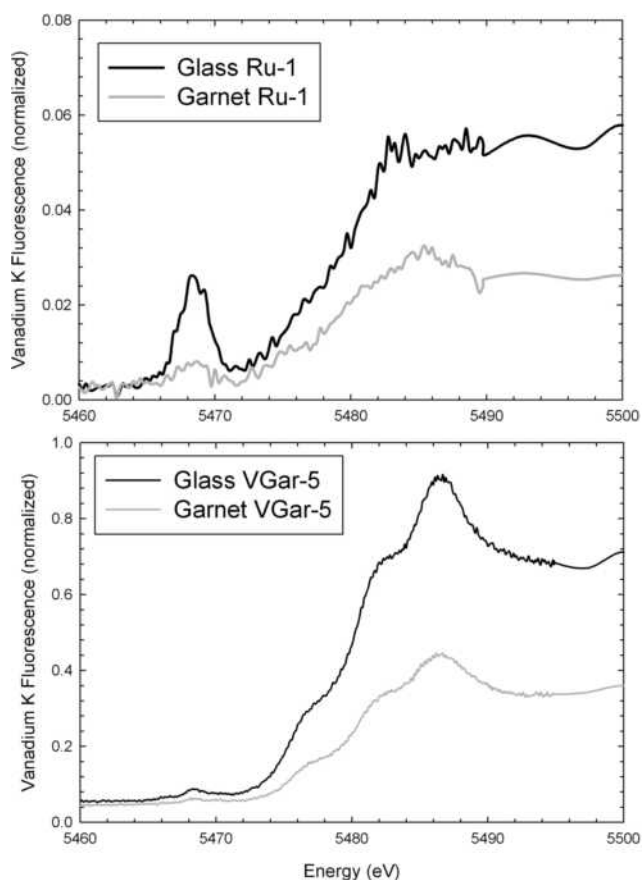


**FIGURE 7.** (a) Normalized intensity across the V K absorption edge, showing the very high pre-edge peak for V in the glass, compared to a smaller peak in the garnet; oxidized experiment (no. 224 at the Ru-RuO<sub>2</sub> buffer). (b) Normalized intensity across the K absorption edge, showing the small pre-edge peak for V in the glass, compared to the very small (or no) peak in the garnet; reduced experiment (no. VGar-5 near IW-1.66).

than in the garnet—the opposite of what is seen at higher  $f_{O_2}$ .

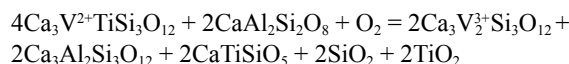
$D(V)$  garnet/melt is greater than 1 at intermediate and low  $f_{O_2}$  ( $\Delta IW = +0.87$ ), but  $<1$  at the highest  $f_{O_2}$  ( $\Delta IW = +9.59$ ; Fig. 6b). More specifically, it seems that V is compatible in garnet if it is mainly in the  $V^{3+}$  or mixed  $V^{3+}$ - $V^{2+}$  states, which means  $f_{O_2}$  less than FMQ buffer. These findings are consistent with the overall compatibility of V in garnet found by previous experimental studies where  $D(V)$  of 1.0 to 3.8 were measured (Hauri et al. 1994; Johnson 1998; Canil 2002; Mallmann and O'Neill 2009). However, a detailed understanding of  $D(V)$  garnet/melt in terms of crystal lattice theory will depend on knowledge of  $f_{O_2}$  and coordination, such as explored by Ohtani et al. (1989) and van Westrenen et al. (2001), although the latter did not include V. Nonetheless, this  $f_{O_2}$  range covers that of the Earth's current and ancient mantle (e.g., Frost and McCammon 2008), Mars (Righter et al. 2008), and even Mercury whose large metallic core and low FeO content crust may imply very low redox conditions (Malavergne et al. 2009).

Average V valence states in garnet from high- $P$  experiments that contain metal and are below the IW buffer (Table 1) are slightly lower than  $3+$ . High-pressure experimental garnets yield a V valence state of  $+2.6$  to  $2.7$ , which may be generally expected for  $f_{O_2}$  slightly lower than IW-2, as estimated from  $X_{FeO}$  and  $X_{Fe}$  (mole fraction of FeO in silicate melt and Fe in metal, respectively) from these experiments.

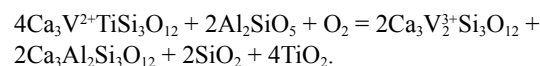
High-pressure megacrystic garnets have V valence state of  $+2.5$  that is generally consistent with other estimates for garnet peridotite (Woodland and Koch 2003; McCammon and Kopylova 2004) that reach values as low as IW, which are at the low end of the range of  $f_{O_2}$  for the terrestrial mantle. Further insight into the valence state of V in natural mantle samples comes from the suite of South African garnets. Despite the variation in  $f_{O_2}$  recorded in this suite ( $\Delta FMQ = -1.8$  to  $-4.5$ ), the V pre-edge peaks indicate a very narrow range of average valence state from 2.46 to 2.55 for all samples and no correlation with  $f_{O_2}$ . So, terrestrial mantle garnets appear to contain a mixture of  $V^{2+}$  and  $V^{3+}$ , but even those coming from more oxidized samples (FMQ-2) have some  $V^{2+}$ , and there is no apparent correlation of V valence state and  $f_{O_2}$ . This suggests that the garnet crystal chemistry is controlling V valence state, and this is a stronger control than oxygen fugacity.

Finally, the natural goldmanite was expected to be trivalent, and was selected with the intention of using it as a standard. However, it yields a lower valence state of 2.56–2.62, suggesting that it contains a mixture of  $V^{2+}$  and  $V^{3+}$ . As discussed in the XRD results section above, including as much as 10% of  $V^{2+}$  improves the agreement between calculated and measured parameters. Although the amount of  $V^{2+}$  is limited by charge-balance constraints, consideration of XANES uncertainty and charge-balance constraints indicate that a small portion (10–40%) of V is divalent. The Czech locality may be more reduced than the experimental garnets produced at FMQ-1 to FMQ-2. Indeed many of the goldmanite localities worldwide (including the Czech locality) are from C-rich black shales or C-rich schists that have high organic carbon contents (e.g., Uher et al. 2008; Jeong and Kim 1999; Benkerrou and Fonteilles 1989). Therefore, a high  $CH_4$  content would favor an environment that is more reduced, and therefore introduce some  $V^{2+}$  that is stable in the garnet structure.

Because  $V^{2+}$  would likely enter garnet's octahedral site, it would require substitution of Ti for Al, perhaps by equilibria such as



or



Either of these equilibria could promote the stability of  $V^{2+}$  in the natural goldmanite because these contain a significant amount (0.075 in the octahedral site) of titanium. The same equilibria written for Si (instead of Ti) could promote the stability of  $V^{2+}$  in the natural mantle garnets, because they come from a depth (3.6 to 6.5 GPa; Woodland and Koch 2003; Peslier et al. 2008) where the majorite component is more significant. The presence of a small amount of  $V^{2+}$  in the experimental and natural garnets in this study can thus be explained by charge balance with either  $Ti^{4+}$  or silicon. The most extreme case is that of the natural goldmanite (discussed above), which has 24 wt%  $V_2O_3$ , but even this example is consistent with some divalent vanadium.

## Chromium

There is no evidence for  $Cr^{2+}$  peaks in any of the spectra obtained in this study. Chromium is trivalent in all experimental garnets (Fig. 8), and natural mantle garnets measured here all yield  $Cr^{3+}$  spectra, even for samples equilibrated at FMQ-4.5. Garnet in the terrestrial mantle will contain trivalent chromium. Although we have measured  $Cr^{3+}$  in our experimental glasses, it is likely that most of the  $Cr^{3+}$  forms upon quenching due to the equilibrium  $Cr^{2+} + Fe^{3+} = Cr^{3+} + Fe^{2+}$  (Berry et al. 2003, 2006; Berry and O'Neill 2004). The experiments of Berry et al. (2006) were quenched rapidly into water, and the experiments of Berry et al. (2003) were done in situ; our glasses were produced at relatively low cooling rates, where the temperature drop from 1300 to 200 °C occurred in approximately 15 s. Berry et al.

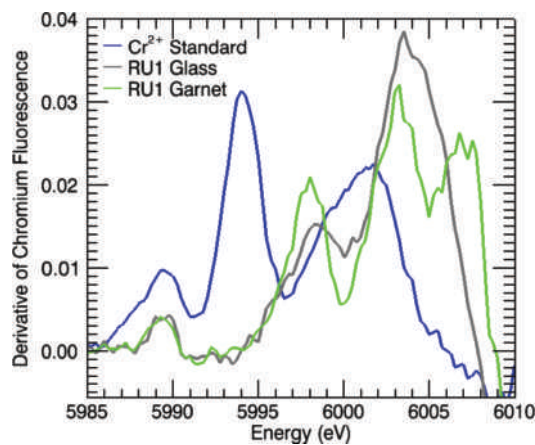


**FIGURE 8.** Chromium XANES spectra for garnet and glass from the most oxidized experiment (224), showing that Cr is  $3+$  in all experimental glasses and garnet studied here; the  $Cr^{2+}$  standard spectrum is shown with its distinctive peak at 5994 eV. (Color online.)

(2006) showed that a significant proportion of Cr in silicate melts is  $\text{Cr}^{2+}$  even at terrestrial mantle  $f_{\text{O}_2}$ . The importance of  $\text{Cr}^{2+}$  in silicate melts becomes more significant at  $f_{\text{O}_2}$  lower than the IW buffer, where metal-bearing systems yield evidence for  $\text{Cr}^{2+}$  (e.g., Wood et al. 2008; Berthet et al. 2009). In addition, Eeckhout et al. (2007) found that  $\text{Cr}^{2+}$  dominates in lower mantle phases such as Mg-perovskite and magnesiowüstite. This demonstrates that the specific valence state of Cr in any given phase must be strongly controlled by crystal chemistry.

The behavior of Cr in garnet/melt pairs contrasts sharply with that of vanadium. The contrasting results for V and Cr can be understood by consideration of crystal field theory. The large octahedral site preference for  $\text{Cr}^{3+}$  in silicates ( $-157.8$  kJ/mol) compared to  $\text{Cr}^{2+}$  ( $-71.1$  kJ/mol) indicates that  $\text{Cr}^{3+}$  will enter octahedral sites very easily (Burns 1993), which is entirely consistent with our results showing  $\text{Cr}^{3+}$  in all garnets measured for this study. On the other hand,  $\text{V}^{3+}$  and  $\text{V}^{2+}$  have nearly identical crystal field splitting energies (Burns 1993), and there may be no preference for one over the other in the garnet structure. This is also consistent with our findings that  $\text{V}^{3+}$  and  $\text{V}^{2+}$  are both measured in garnets across a wide range of oxygen fugacities (e.g., Wänke 1981).

### Terrestrial mantle

The V and Cr contents of Earth's primitive upper mantle have been the subject of considerable debate over the last three decades. Because they are compatible in deep mantle phases, and also exhibit siderophile behavior, their concentrations in the mantle have been attributed to both core formation (e.g., Wood et al. 2008) and deep mantle fractionation (e.g., Kato et al. 1988). In fact, both are likely to be important depending on the details of the models being considered. For example, V is compatible in garnet and other deep mantle silicates and oxides, and prefers these phases to metal, but at very low oxygen fugacities—less than approximately IW-3—V becomes compatible in metal (Fig. 9). For a few of these phases (garnet and pyroxene),  $\text{V}^{3+}$  is the stable dominant valence state, whereas for other deep mantle phases, the valence state is not known but may be a mixture of divalent and trivalent cations. In this section, we compare the relative compatibilities of V and Cr in these phases at high pressure and temperature conditions, and suggest that for the Earth, compatibility of V and Cr in deep mantle silicates and oxides is just as important as the core-forming metal.

Metal-silicate partition coefficients for siderophile elements like V and Cr during core formation will change as a function of pressure, temperature, oxygen fugacity, valence state, and metal and silicate composition. Calculation of metal-silicate partition coefficients as a function of all these variables has been possible using an approach guided by chemical thermodynamics where:

$$\ln D(\text{met/sil}) = a \ln f_{\text{O}_2} + b/T + cP/T + d \ln(1 - X_{\text{S}}) + e \ln(1 - X_{\text{C}}) + f[\text{NBO}/T] + g[\text{S}] + h. \quad (1)$$

The  $a$ ,  $b$ ,  $c$ , and  $h$  terms relate to valence state, enthalpy ( $H/RT$ ), volume ( $VP/RT$ ), and entropy ( $S/R$ ), respectively, the  $d$  and  $e$  terms relate to activity expressions for these elements in a metallic liquid ( $X_{\text{S}}$  and  $X_{\text{C}}$  = mole fraction of S and C in the metallic liquid, respectively), the  $f$  terms relate to silicate melt structure and are

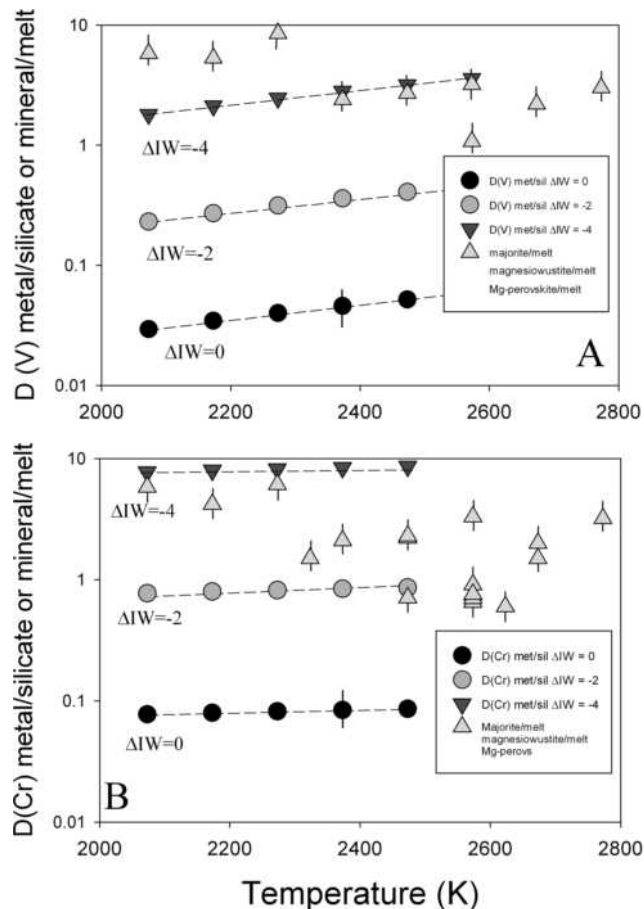


**FIGURE 9.** (a and b) Vanadium and Cr are compatible in garnet and other silicates and oxides, and prefer these phases to metal, except at very low oxygen fugacities—less than IW-3. Metal-silicate partition coefficients for Cr and V are calculated using the approach in the text, and regression coefficients and  $2\sigma$  error in Figure 10. Specific conditions are 25 GPa, primitive upper mantle (NBO/T = 2.8 and S content of 200 ppm), metallic core composition of  $X_{\text{S}} = 0.1$  and  $X_{\text{C}} = 0.05$ , and variable relative  $f_{\text{O}_2}$  and temperature. Oxygen fugacity of the mineral/melt partitioning experiments is typically between IW and IW-2. Predictive equations of Wood et al. (2008) and Chabot and Agee (2003) predict even lower values of  $D(\text{metal/silicate})$  at each given relative  $f_{\text{O}_2}$ , making the point even stronger that the deep mantle phases are the major hosts for these three elements and must be quantified and accounted for in any differentiation model. Mg-perovskite/melt data are from Ohtani et al. (1995), Taura et al. (2001), Kato et al. (1996), McFarlane et al. (1994), Liebske et al. (2005), and Corgne et al. (2005). Magnesiowüstite/melt data are from Gessmann and Rubie (1998), Agee (1993), McFarlane (1994), McFarlane et al. (1994), and Ohtani and Yurimoto (1996). Garnet/melt data are from Trønnes et al. (1992), Kato et al. (1988), McFarlane (1994), Yurimoto and Ohtani (1992), and Drake et al. (1993). Error on partition coefficients are given as 10%, which is typical for values determined using various analytical approaches. It is likely that the mantle depletions (relative to chondrites) of V and Cr are due to silicates and oxides in the deep mantle as well as to metal in the core.

regressed against NBO/T, as defined by Mysen (1991) and Mills (1993) (e.g., Righter et al. 1997; Walter and Thibault 1995), and the  $g$  terms relate to the S content of the silicate melt (in ppm).

Vanadium and Cr partition coefficients [ $D(\text{V})$  and  $D(\text{Cr})$  metal/silicate] from several different studies can be combined to

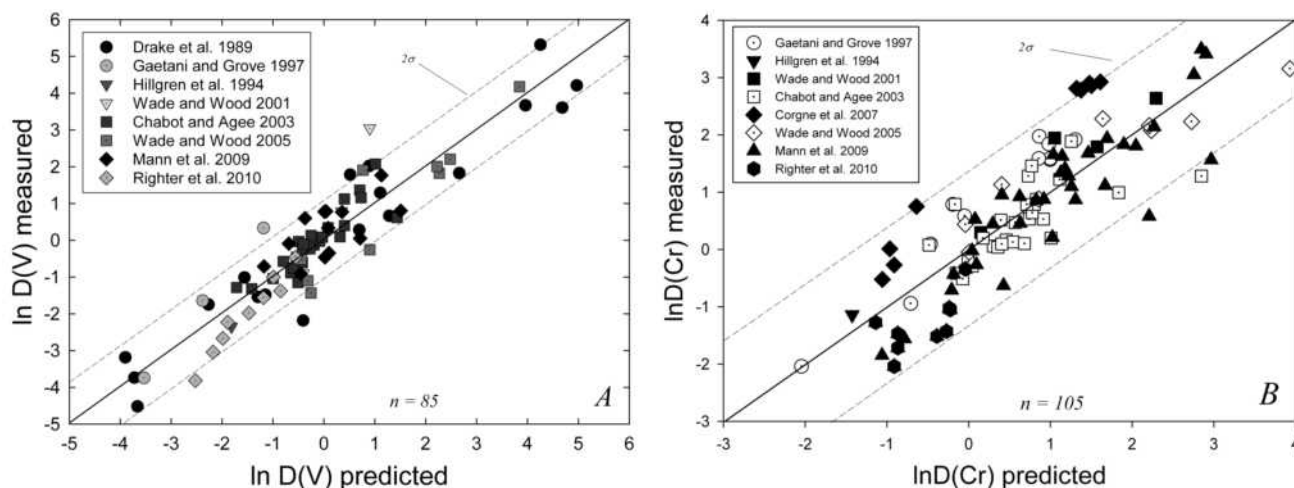


**FIGURE 10.** (a) Comparison of measured and predicted  $\ln D(V)$  from the multiple linear regression analysis using data sets of Drake et al. (1989), Gaetani and Grove (1997), Hillgren et al. (1994), Wade and Wood (2001, 2005), Chabot and Agee (2003), Mann et al. (2009), and Righter et al. (2010). Regression coefficients (for Eq. 1) are  $a = -0.45(0.03)$ ;  $b = -35\,800(2280)$ ;  $c = 575(56)$ ;  $d = -5.63(0.48)$ ;  $e = -3.86(0.84)$ ;  $f = -0.41(0.06)$ ;  $g = -0.000152(79)$ ; and  $h = 8.08(0.83)$ . Number of data points is 85,  $r^2 = 0.881$ , and standard error is 0.71. (b) Comparison of measured and predicted  $\ln D(Cr)$  from the multiple linear regression analysis using data sets of Gaetani and Grove (1997), Hillgren et al. (1994), Wade and Wood (2001, 2005), Chabot and Agee (2003), Mann et al. (2009), Corgne et al. (2007), and Righter et al. (2010). Regression coefficients (for Eq. 1) are  $a = -0.50(0.03)$ ;  $b = -33\,490(2330)$ ;  $c = 652(56)$ ;  $d = -6.49(0.57)$ ;  $e = -2.94(0.59)$ ;  $f = -0.30(0.06)$ ; and  $h = 6.66(0.75)$ . Number of data points is 105,  $r^2 = 0.823$ , and standard error is 0.69.

derive regression coefficients  $a$  through  $g$  for a predictive expression (Figs. 10a and 10b). The studies of Drake et al. (1989) and Gaetani and Grove (1997) illustrate the effects of  $f_{O_2}$ , Hillgren et al. (1994), Wade and Wood (2001, 2005), and Mann et al. (2009) the effects of pressure, and the studies of Chabot and Agee (2003) and Righter et al. (2010) the effects of temperature. The effects of variable melt composition were analyzed by Righter et al. (2010) for a sequence of basalt to peridotite.

If the Cr and V depletions were to be explained entirely by core formation, the required  $D(Cr)$  metal/silicate and  $D(V)$  metal/silicate would be 2.9–3.4 and 1.83, respectively (Allegre et al. 1995; McDonough and Sun 1995). Using the newly derived expressions and a fixed primitive mantle composition (primitive upper mantle of McDonough and Sun 1995, with 200 ppm S) and core composition ( $X_s = 0.1$  and  $X_c = 0.05$  for illustrative purposes), we can calculate the values of  $D(Cr)$  and  $D(V)$  as a function of  $f_{O_2}$  and temperature (at 25 GPa) to show the relative compatibility of Cr and V in metal vs. deep mantle oxides and silicates. It is clear from the calculations that  $D(Cr)$  metal/silicate and  $D(V)$  metal/silicate remain  $<1$  unless the oxygen fugacity is very low. In fact,  $D(V)$  and  $D(Cr)$  are always higher for deep mantle phases unless the  $f_{O_2}$  is as low as IW-3 or IW-4, where metal is the major host. Given this compatibility, it is likely that the mantle depletions (relative to chondrites) of V and Cr are due both to silicates and oxides in the deep mantle as well as to metal in the core (Fig. 9). Only at oxygen fugacities lower than IW-3 or IW-4 would  $D(V)$  and  $D(Cr)$  metal/silicate be higher than those for silicates or oxides. But at these low  $f_{O_2}$ , there will be much lower FeO in the Earth's primitive mantle, so this is unrealistic. Furthermore, it is likely that  $f_{O_2}$  has been underestimated in high-pressure experiments (Righter and Ghiorso 2009), and if anything is higher and therefore  $D(\text{metal/silicate})$  will be even lower for V and Cr.

Finally, consideration of crystal field theory helps to explain the tendency for Cr and V to be compatible in ferripericlase and Mg-perovskite. Both of these cations maintain high octahedral site preference energies and both of these mineral structures have octahedral sites at high pressures (e.g., Burns 1993).

#### Variable Sc/V in mantle garnets

Sc/V ratios in mantle garnets are variable and correlate well with calculated equilibration temperatures (Canil et al. 2003; Scully et al. 2004). Several factors could cause such variations, including temperature, oxygen fugacity, pressure, or a change in V valence state. Our results can place some constraints on the cause of this variation. Because V valence state does not seem to be connected to variation in oxygen fugacity, valence state can be ruled out as a controlling factor. However, oxygen fugacity is linked to the magnitude of the partition coefficient between garnet and silicate melt,  $D(V)$  garnet/melt (Fig. 6b). Vanadium is only mildly compatible at high  $f_{O_2}$ , but becomes much more compatible at  $f_{O_2}$  near IW buffer, whereas the magnitude of  $D(Sc)$  garnet/melt is constant and independent of  $f_{O_2}$ . Studies of  $f_{O_2}$  of garnet-bearing peridotites from Africa have shown that the deepest peridotites are also the most reduced (Woodland and Koch 2003; Lazarov et al. 2009). It is possible that the trend of lower Sc/V garnets at higher temperatures is caused by the generation of the low Sc/V garnets at deeper, hotter, and more reduced conditions. Under such conditions, V would be retained in garnet, thus giving the garnet a lower Sc/V ratio. Sc/V ratios would increase at lower  $PT$  conditions, where  $f_{O_2}$  is slightly higher and therefore  $D(V)$  garnet/melt is slightly lower, leaving the garnet with less V (but same amount of Sc) than the deeper garnets. This idea must be tested with more systematic study of the dependence of  $D(V)$  and  $D(Sc)$  with temperature and pressure, to assess the importance of variations in these intensive variables.

### CONCLUDING REMARKS

Our new results have four fundamental implications for the high-temperature mantle geochemistry of V and Cr. First, with the variation of oxygen fugacity, the average valence state of V is variable in garnets between 2+ and 4+, but was not measured any lower than 2.5, even for mantle samples equilibrated near the IW buffer. This indicates that  $f_{O_2}$  is the controlling factor in determining V valence state in natural mantle garnets at  $f_{O_2} > \text{FMQ}$ . Below FMQ, the valence state may instead be controlled by garnet crystal chemistry and major and minor element substitutions between Si or Ti and Al. This observation unfortunately indicates that V may not be used to infer  $f_{O_2}$  conditions from garnet-bearing mantle samples. Second, the valence state is nearly constant at 3+ for Cr in garnets and oxidized (>IW) glasses, which contrasts with many other mantle phases that show evidence for incorporation of  $\text{Cr}^{2+}$  in their structures at  $f_{O_2}$  relevant to the terrestrial mantle. Third, the valence state of V is always higher in glass than in coexisting garnets, except possibly at very low  $f_{O_2}$  where silicate melt may have lower valence state than the coexisting garnet. This means that several valence states of V may coexist in any given system, depending upon the phases present. Fourth, both V and Cr exhibit small depletions in the terrestrial mantle. These elements could be hosted in deep mantle phases as well as in the core liquid metal (Fig. 9). This possibility is relevant to both the terrestrial and martian mantles (Righter and Chabot 2010; Righter 2011) as well as the Moon, which may harbor deep mantle garnet (e.g., Neal 2001).

### ACKNOWLEDGMENTS

Portions of this work were performed at GeoSoilEnviroCARS (Sector 13), Advanced Photon Source (APS), Argonne National Laboratory. GeoSoilEnviroCARS is supported by the National Science Foundation, Earth Sciences (EAR-0622171) and Department of Energy, Geosciences (DE-FG02-94ER14466). Use of the Advanced Photon Source was supported by the U.S. Department of Energy, Office of Science, Office of Basic Energy Sciences, under Contract No. DE-AC02-06CH11357. Research at JSC was supported by a RTOP to K.R. from the NASA Cosmochemistry program. Some travel was supported by the Lunar and Planetary Institute. We thank D. Schulze and D. Canil for guidance in finding literature mantle garnet analyses, and E.J. Essene for discussions relating to site substitutions. A. Peslier, A. Woodland, and M. Lazarov kindly provided a suite of well-characterized natural garnets from South African mantle xenoliths. B. Hanson and J. Jones made the Cr glass standards, and A. Martin assisted with the XANES analysis. Helpful reviews by T. Mikouchi, D. Canil, and Associate Editor M.D. Dyar are appreciated and contributed to the clarity of the presentation.

### REFERENCES CITED

- Agee, C.B. (1993) High pressure melting of carbonaceous chondrite. *Journal of Geophysical Research*, 98, 5419–5426.
- Allegre, C.J., Poirier, J.-P., Humler, E., and Hofmann, A.W. (1995) The chemical composition of the Earth. *Earth and Planetary Science Letters*, 134, 515–526.
- Bajt, S., Sutton, S.R., and Delaney, J.S. (1994) X-ray microprobe analysis of iron oxidation states in silicates and oxides using X-ray absorption near edge structure (XANES). *Geochimica et Cosmochimica Acta*, 58, 5209–5214.
- Benkerrou, C. and Fontilles, M. (1989) Vanadium garnets in calcareous metapelites and skarns at Coat-an Noz, Belle-Isle-en-Terre (Côtes du Nord), France. *American Mineralogist*, 74, 852–858.
- Berry, A.J. and O'Neill, H.St.C. (2004) A XANES determination of the oxidation state of chromium in silicate glasses. *American Mineralogist*, 89, 790–798.
- Berry, A.J., Shelley, J.M.G., Foran, G.J., O'Neill, H.St.C., and Scott, D.R. (2003) A furnace design for XANES spectroscopy of silicate melts under controlled oxygen fugacities and temperatures to 1773 K. *Journal of Synchrotron Radiation*, 10, 332–336.
- Berry, A.J., O'Neill, H.St.C., Scott, D.R., Foran, G.J., and Shelley, J.M.G. (2006) The effect of composition on  $\text{Cr}^{2+}/\text{Cr}^{3+}$  in silicate melts. *American Mineralogist*, 91, 1901–1908.
- Berthet, S. (2009) Métamorphisme d'une chondrite à enstatite nommée Indarch: implications sur les phénomènes de différenciation planétaire. Application à la Terre, 235 pp. Ph.D. thesis, Université Paris-Est Ecole Doctoral Mode.
- Berthet, S., Malavergne, V., Corgne, A., Righter, K., and Combes, R. (2006) The evolution of the EH4 chondrite Indarch at high pressure and temperature: the first experimental results. *Lunar and Planetary Science*, XXXVII, 2026.
- Berthet, S., Malavergne, V., and Righter, K. (2009) Melting of the Indarch meteorite (EH4 chondrite) at 1 GPa and variable oxygen fugacity: Implications for early planetary differentiation processes. *Geochimica et Cosmochimica Acta*, 73, 6402–6420.
- Burns, R.G. (1993) *Mineralogical Applications of Crystal Field Theory*. Cambridge University Press, U.K.
- Canil, D. (2002) Vanadium in peridotites, mantle redox and tectonic environments: Archean to present. *Earth and Planetary Science Letters*, 195, 75–90.
- Canil, D. and Wei, K. (1992) Constraints on the origin of mantle-derived low Ca garnets. *Contributions to Mineralogy and Petrology*, 109, 421–430.
- Canil, D., Schulze, D.J., Hall, D., Hearn, B.C. Jr., and Milliken, S.M. (2003) Lithospheric roots beneath western Laurentia: the geochemical signal in mantle garnets. *Canadian Journal of Earth Science*, 40, 1027–1051.
- Chabot, N.L. and Agee, C.B. (2003) Core formation in the Earth and Moon: new experimental constraints from V, Cr, and Mn. *Geochimica et Cosmochimica Acta*, 67, 2077–2091.
- Channon, M., Garber, J., Danielson, L.R., and Righter, K. (2007) Liquid Phases of the Richardton H5 Chondrite at High Pressures and Temperatures. 38th Lunar and Planetary Science Conference. LPI Contribution No. 1338, p. 1456.
- Chou, I.M. (1987) Oxygen buffer and hydrogen sensor techniques at elevated pressures and temperatures. In G.C. Ulmer and H.L. Barnes, Eds., *Hydrothermal Experimental Techniques*, p. 61–99. Wiley, New York.
- Corgne, A., Liebske, C., Wood, B.J., Rubie, D.C., and Frost, D.J. (2005) Silicate perovskite-melt partitioning of trace elements and geochemical signature of a deep perovskite reservoir. *Geochimica et Cosmochimica Acta*, 69, 485–496.
- Corgne, A., Keshav, S., Wood, B.J., McDonough, W.F., and Fei, Y. (2007) Metal-silicate partitioning and constraints on core composition and oxygen fugacity during Earth accretion. *Geochimica et Cosmochimica Acta*, 72, 574–589.
- Cygan, R.T. and Lasaga, A.C. (1985) Self-diffusion of magnesium in garnet at 750° to 900 °C. *American Journal of Science*, 285, 328–350.
- Drake, M.J., Newsom, H., and Capobianco, C.J. (1989) V, Cr, and Mn in the earth, moon, EPB, and SPB and the origin of the moon—Experimental studies. *Geochimica et Cosmochimica Acta*, 53, 2101–2111.
- Drake, M.J., McFarlane, E.A., Gasparik, T., and Rubie, D.C. (1993) Mg-perovskite/silicate melt and majorite garnet/silicate melt partition coefficients in the system CaO-MgO-SiO<sub>2</sub> at high temperatures and pressures. *Journal of Geophysical Research*, 98, 5427–5431.
- Eeckhout, S.G., Bolfan-Casanov, N., McCammon, C., Klemme, S., and Amiguet, E. (2007) XANES study of the oxidation state of Cr in lower mantle phases: Periclase and magnesium silicate perovskite. *American Mineralogist*, 92, 966–972.
- Filiberto, J., Treiman, A.H., and Le, L. (2008) Crystallization experiments on a Gusev basalt composition. *Meteoritics and Planetary Science*, 43, 1137–1146.
- French, B.M. and Eugster, H.P. (1965) Experimental control of oxygen fugacities by graphite-gas equilibria. *Journal of Geophysical Research*, 70, 1529–1539.
- Frost, D.J. and McCammon, C.A. (2008) The redox state of Earth's mantle. *Annual Review of Earth and Planetary Sciences*, 36, 389–420.
- Frost, D.J. and Wood, B.J. (1997) Experimental measurements of the fugacity of CO<sub>2</sub> and graphite/diamond stability from 35 to 77 kbar at 925 to 1650°C. *Geochimica et Cosmochimica Acta*, 61, 1565–1574.
- Gaetani, G. and Grove, T.L. (1997) Partitioning of moderately siderophile elements among olivine, silicate melt, and sulfide melt: Constraints on core formation in the Earth and Mars. *Geochimica et Cosmochimica Acta*, 61, 1829–1846.
- Gessmann, C.K. and Rubie, D.C. (1998) The effect of temperature on the partitioning of nickel, cobalt, manganese, chromium and vanadium at 9 GPa and constraints on formation of the Earth's core. *Geochimica et Cosmochimica Acta*, 62, 867–882.
- Gessmann, C.K., Rubie, D.C., and McCammon, C.A. (1999) Oxygen fugacity dependence of Ni, Co, Mn, Cr, V, and Si partitioning between liquid metal and magnesiowüstite at 9–18 GPa and 2200°C. *Geochimica et Cosmochimica Acta*, 63, 1853–1863.
- Gunsser, W., Lemke, Th., Rohl, B.R., and Denecke, M.A. (1994) X-ray absorption spectroscopic and magnetic investigations on the garnet  $\text{Mn}_3\text{Al}_{2-x}\text{Cr}_x\text{Ge}_2\text{O}_{12}$ . *Journal of Solid State Chemistry*, 118, 261–266.
- Hanson, B. and Jones, J.H. (1998) The systematics of  $\text{Cr}^{3+}$  and  $\text{Cr}^{2+}$  partitioning between olivine and liquid in the presence of spinel. *American Mineralogist*, 83, 669–684.
- Hauri, E.H., Wagner, T.P., and Grove, T.L. (1994) Experimental and natural partitioning of Th, U, Pb and other trace elements between garnet, clinopyroxene, and basaltic melts. *Chemical Geology*, 117, 149–166.
- Hillgren, V.J., Drake, M.J., and Rubie, D.C. (1994) High-pressure and high-temperature experiments on core-mantle segregation in the accreting Earth. *Science*, 264, 1442–1445.
- Jeong, G.Y. and Kim, Y.H. (1999) Goldmanite from the black slates of the Ogcheon

- belt, Korea. *Mineralogical Magazine*, 63, 253–256.
- Johnson, K.T.M. (1998) Experimental determination of partition coefficients for rare earth and high field strength elements between clinopyroxene, garnet, and basaltic melt at high pressures. *Contributions to Mineralogy and Petrology*, 133, 60–68.
- Karner, J.M., Papike, J.J., Sutton, S.R., Shearer, C.K., McKay, G.A., Le, L., and Burger, P. (2007) Valence state partitioning of Cr between pyroxene-melt: Effects of pyroxene and melt composition and direct determination of Cr valence states by XANES: Application to Martian basalt QUE 94201 composition. *American Mineralogist*, 92, 2002–2005.
- Kato, T., Ringwood, A.E., and Irifune, T. (1988) Experimental determination of element partitioning between silicate perovskites, garnets and liquids: constraints on early differentiation of the mantle. *Earth and Planetary Science Letters*, 89, 123–145.
- Kato, T., Ohtani, E., Ito, Y., and Onuma, K. (1996) Element partitioning between silicate perovskites and calcic ultrabasic melt. *Physics of the Earth and Planetary Interiors*, 96, 201–207.
- Lazarov, M., Woodland, A.B., and Brey, G. (2009) Thermal state and redox conditions of the Kaapvaal mantle: a study of xenoliths from the Finsch Mine, South Africa. *Lithos*, 112, 913–923.
- Liebske, C., Corgne, A., Frost, D.J., Rubie, D.C., and Wood, B.J. (2005) Compositional effects on element partitioning between Mg-silicate perovskite and silicate melts. *Contributions to Mineralogy Petrology*, 149, 113–128.
- Malavergne, V., Toplis, M.J., Berthet, S., and Jones, J. (2009) Highly reducing conditions during core formation on Mercury: Implications for internal structure and the origin of a magnetic field. *Icarus*, 206, 199–210.
- Mallmann, G. and O'Neill, H.St.C. (2009) The crystal/melt partitioning of V during mantle melting as a function of oxygen fugacity compared with some other elements (Al, P, Ca, Sc, Ti, Cr, Fe, Ga, Y, Zr and Nb). *Journal of Petrology*, 50, 1765–1794.
- Mann, U., Frost, D.J., and Rubie, D.C. (2009) Evidence for high-pressure core-mantle differentiation from the metal-silicate partitioning of lithophile and weakly siderophile elements. *Geochimica et Cosmochimica Acta*, 73, 7360–7386.
- McCammon, C. and Kopylova, M.G. (2004) A redox profile of the Slave mantle and oxygen fugacity control in the cratonic mantle. *Contributions to Mineralogy Petrology*, 148, 55–68.
- McDonough, W.F. and Sun, S.-s. (1995) The composition of the Earth. *Chemical Geology*, 120, 223–254.
- McFarlane, E.A. (1994) Differentiation in the early Earth: an experimental investigation. Ph.D. thesis, University of Arizona, Tucson.
- McFarlane, E.A., Drake, M.J., and Rubie, D.C. (1994) Element partitioning between Mg-perovskite, magnesio-wüstite, and silicate melt at conditions of the Earth's mantle. *Geochimica et Cosmochimica Acta*, 58, 5161–5172.
- Médard, E., McCammon, C.A., Barr, J.A., and Grove, T.L. (2008) Oxygen fugacity, temperature reproducibility, and H<sub>2</sub>O content for nominally anhydrous piston-cylinder experiments using Pt-graphite capsules. *American Mineralogist*, 93, 1838–1844.
- Mills, K.C. (1993) The influence of structure on the physico-chemical properties of slags. *ISIJ International*, 33, 148–155.
- Moench, R.H. and Meyrowitz, R. (1964) Goldmanite, a vanadium garnet from Laguna, New Mexico. *American Mineralogist*, 49, 644–655.
- Mysen, B.O. (1991) Volatiles in magmatic liquids. In L.L. Perchuk and I. Kushiro, Eds., *Physical Chemistry of Magma*, p. 435–476. Cambridge University Press, New York.
- Neal, C.R. (2001) The interior of the Moon: The presence of garnet in the primitive, deep lunar mantle. *Journal of Geophysical Research*, 106, 27865–27885.
- Novak, G.A. and Gibbs, G.V. (1971) The crystal chemistry of the silicate garnet. *American Mineralogist*, 56, 791–825.
- O'Hara, M.J. and Mercy, E.L.P. (1966) Eclogite, peridotite and pyrope from the Navajo country, Arizona and New Mexico. *American Mineralogist*, 51, 336–352.
- O'Neill, H.St.C. (1986) Mo-MoO<sub>2</sub> (MOM) oxygen buffer and the free energy of formation of MoO<sub>2</sub>. *American Mineralogist*, 71, 1007–1010.
- (1987) Quartz-fayalite-iron and quartz-fayalite-magnetite equilibria and the free energy of formation of fayalite and magnetite. *American Mineralogist*, 72, 67–75.
- O'Neill, H.St.C. and Nell, J. (1997) Gibbs free energy of formation of RuO<sub>2</sub>, IrO<sub>2</sub>, and OsO<sub>2</sub>: a high temperature electrochemical and calorimetric study. *Geochimica et Cosmochimica Acta*, 61, 5279–5293.
- Ohtani, E. and Yurimoto, H. (1996) Element partitioning between metallic liquid, magnesio-wüstite and silicate liquid at 20 GPa and 2500 °C: A SIMS study. *Geophysical Research Letters*, 23, 1993–1996.
- Ohtani, E., Yurimoto, H., Segawa, T., and Kato, T. (1995) Element partitioning between MgSiO<sub>3</sub> perovskite, magma, and molten iron: constraints for the earliest processes of the Earth-Moon system. In T. Yukutake, Ed., *The Earth's Central Part: Its Structure and Dynamics*, p. 287–300. Terra Scientific, Tokyo.
- Ohtani, E., Kawabe, I., Moriyama, J., and Nagata, Y. (1989) Partitioning of elements between majorite garnet and melt and implications for petrogenesis of komatiite. *Contributions to Mineralogy Petrology*, 103, 263–269.
- Osana, Y., Ueno, T., Tsuchiya, N., Takahashi, Y., Tainosho, Y., and Shiraishi, K. (1990) Finding of vanadium-bearing garnet from the Sor Rondane Mountains, East Antarctica. *Antarctic Record*, 34, 279–291.
- Pan, Y. and Fleet, M.E. (1992) Mineral chemistry and geochemistry of vanadian silicates in the Hemlo gold deposit, Ontario, Canada. *Contributions to Mineralogy Petrology*, 109, 511–525.
- Peslier, A.H., Woodland, A.B., and Wolff, J.A. (2008) Fast kimberlite ascent rates estimated from hydrogen diffusion profiles in xenolithic mantle olivines from southern Africa. *Geochimica et Cosmochimica Acta*, 72, 2711–2722.
- Pouchou, J.-L. and Pichoir, F. (1991) Quantitative analysis of homogeneous or stratified microvolumes applying the model "PAP." In K.F.J. Heinrich and D.E. Newbury, Eds., *Electron Microprobe Quantitation*, p. 31–75. Plenum Press, New York.
- Righter, K. (2011) Prediction of metal-silicate partition coefficients for siderophile elements: an update and assessment of PT conditions for metal-silicate equilibrium during accretion of the Earth. *Earth and Planetary Science Letters*, 304, 158–167.
- Righter, K. and Chabot, N.L. (2010) Siderophile element constraints on the depth and extent of melting on early Mars. *Meteoritics and Planetary Science*, 46, 157–176.
- Righter, K. and Ghiorso, M. (2009) Calculation of oxygen fugacity in high pressure metal-silicate experiments and comparison to standard approaches. Workshop in Experiments and Modeling in Cosmochemistry, Nancy, France, July 2009.
- Righter, K. and Shearer, C.K. (2003) Magmatic Fractionation of Hf and W: Constraints on the timing of core formation and differentiation in the Moon and Mars. *Geochimica et Cosmochimica Acta*, 67, 2497–2507.
- Righter, K., Drake, M.J., and Scott, E.R.D. (2006a) Compositional relationships between meteorites and terrestrial planets. In D. Lauretta and H.Y. McSween, Jr., Eds., *Meteorites and the Early Solar System*, p. 803–828. University of Arizona Press, Tucson.
- Righter, K., Sutton, S.R., Newville, M., Le, L., Schwandt, C.S., Uchida, H., Lavina, B., and Downs, R.T. (2006b) An experimental study of the oxidation state of vanadium in spinel and basaltic melt with implications for the origin of planetary basalt. *American Mineralogist*, 91, 1643–1658.
- Righter, K., Yang, H., Costin, G., and Downs, R.T. (2008) Oxygen fugacity in the Martian mantle controlled by carbon: New constraints from the nakhlite MIL 03346. *Meteoritics and Planetary Science*, 43, 1709–1723.
- Righter, K., Pando, K., and Danielson, L.R. (2009) Experimental evidence for sulfur-rich martian magmas: Implications for volcanism and surficial sulfur sources. *Earth and Planetary Science Letters*, 288, 235–243.
- Righter, K., Pando, K., Danielson, L.R., and Lee, C.T. (2010) Partitioning of Mo, P and other siderophile elements (Cu, Ga, Sn, Ni, Co, Cr, Mn, V, W) between metal and silicate melt as a function of temperature and silicate melt composition. *Earth and Planetary Science Letters*, 291, 1–9.
- Righter, K., Drake, M.J., and Yaxley, G. (1997) Prediction of siderophile element metal-silicate partition coefficients to 20 GPa and 2800 °C: the effect of pressure, temperature, *f*<sub>O<sub>2</sub></sub> and silicate and metallic melt composition. *Physics of the Earth Planetary Interiors*, 100, 115–134.
- Robie, R.A., Hemingway, B.S., and Fisher, J.R. (1978) Thermodynamic properties of minerals and related substances at 298.15 K and 1 bar (10<sup>5</sup> pascals) pressure and at higher temperatures. U.S. Geological Survey Bulletin, 1452, 456 p.
- Roden, M.F. and Shimizu, N. (2000) Trace element abundances in mantle-derived minerals which bear on compositional complexities in the lithosphere of the Colorado Plateau. *Chemical Geology*, 165, 283–305.
- Schreiber, H.D., Merkel, R.C. Jr., Schreiber, V.L., and Balazs, G.B. (1987) Mutual interactions of redox couples via electron exchange in silicate melts: models for geochemical melt systems. *Journal of Geophysical Research*, 92, 9233–9245.
- Schulze, D.J., Canil, D., Channer, D.M.D., and Kaminsky, F.V. (2006) Layered mantle structure beneath the western Guyana Shield, Venezuela: Evidence from diamonds and xenocrysts in Guianamo kimberlites. *Geochimica et Cosmochimica Acta*, 70, 192–205.
- Scully, K.R., Canil, D., and Schulze, D.J. (2004) The lithospheric mantle of the Archean Superior Province as imaged by garnet xenocryst geochemistry. *Chemical Geology*, 207, 189–221.
- Shannon, R.D. (1976) Revised effective ionic radii and systematic studies of interatomic distances in halides and chalcogenides. *Acta Crystallographica*, A32, 751–760.
- Sheldrick, G.M. (2008) A short history of SHELX. *Acta Crystallographica*, A64, 112–122.
- Shimizu, N. and Allegre, C.J. (1978) Geochemistry of transition elements in garnet ilherzolite nodules in kimberlites. *Contributions to Mineralogy Petrology*, 67, 41–50.
- Shulman, R.G., Yafet, Y., Eisenberger, P., and Blumberg, W.E. (1976) Observation and interpretation of X-ray absorption edges in iron compounds and proteins. *Proceedings of the National Academy of Sciences*, 73, 1384–1388.
- Sitepu, H., Kopylova, M.G., Quirt, D.H., Cutler, J.N., and Kotzer, T.G. (2005) Synchrotron micro-X-ray fluorescence analysis of natural diamonds: first steps in identification of mineral inclusions in situ. *American Mineralogist*, 90, 1740–1747.

- Snetsinger, K.G., Bunch, T.E., and Keil, K. (1968) Electron microprobe analysis of vanadium in the presence of titanium. *American Mineralogist*, 53, 1770–1773.
- Strens, R.G.J. (1965) Synthesis and properties of calcium vanadium garnet (goldmanite). *American Mineralogist*, 50, 260.
- Sutton, S.R., Bertsch, P.M., Newville, M., Rivers, M., Lanzirotti, A., and Eng, P. (2002) Microfluorescence and Microtomography Analyses of Heterogeneous Earth and Environmental Materials. In P. Fenter, M. Rivers, N. Sturchio, and S. Sutton, Eds., *Applications of Synchrotron Radiation in Low-temperature Geochemistry and Environmental Sciences*, 49, p. 429–483. Reviews on Mineralogy and Geochemistry, Mineralogical Society of America, Chantilly, Virginia.
- Sutton, S.R., Jones, K.W., Gordon, B., Rivers, M.L., Bajt, S., and Smith, J.V. (1993) Reduced chromium in olivine grains from lunar basalt 15555—X-ray absorption near edge structure (XANES). *Geochimica et Cosmochimica Acta*, 57, 461–468.
- Sutton, S.R., Karner, J., Papike, J., Delaney, J.S., Shearer, C., Newville, M., Eng, P., Rivers, M., and Dyar, M.D. (2005) Vanadium K edge XANES of synthetic and natural basaltic glasses and application to microscale oxygen barometry. *Geochimica et Cosmochimica Acta*, 69, 2333–2348.
- Switzer, G.S. (1977) Mineral sciences investigations. *Smithsonian Contributions to the Earth Sciences*, 19, 1–21.
- Taura, H., Yurimoto, H., Kato, T., and Sueno, S. (2001) Trace element partitioning between silicate perovskites and ultracalcic melt. *Physics of the Earth and Planetary Interiors*, 124, 25–32.
- Trønnes, R.G., Canil, D., and Wei, K. (1992) Element partitioning between silicate minerals and coexisting melts at pressures of 1–27 GPa, and implications for mantle evolution. *Earth and Planetary Science Letters*, 111, 241–255.
- Uher, P., Kovacek, M., Kubis, M., Shtukenberg, A., and Ozdin, D. (2008) Metamorphic vanadian-chromian silicate mineralization in carbon-rich amphibole schists from the Male Karpaty Mountains, western Carpathians, Slovakia. *American Mineralogist*, 93, 63–73.
- van Westrenen, W., Wood, B.J., and Blundy, J.D. (2001) A predictive thermodynamic model of garnet-melt trace element partitioning. *Contributions to Mineralogy Petrology*, 142, 219–234.
- Wade, J. and Wood, B.J. (2001) The Earth's “missing” niobium may be in the core. *Nature*, 409, 75–78.
- (2005) Core formation and the oxidation state of the Earth. *Earth and Planetary Science Letters*, 236, 78–95.
- Walter, M.J. and Thibault, Y. (1995) Partitioning of tungsten and molybdenum between metallic liquid and silicate melt. *Science*, 270, 1186–1189.
- Wänke, H. (1981) Constitution of terrestrial planets. *Philosophical Transactions of the Royal Society (London)*, Series A, 303, 287–301.
- Waychunas, G.A., Apter, M.J., and Brown, G.E. Jr. (1983) X-ray K-edge absorption spectra of Fe minerals and model compounds: near-edge structure. *Physics and Chemistry of Minerals*, 10, 1–9.
- Wong, J., Lytle, F.W., Messmer, R.P., and Maylotte, D.H. (1984) K-edge absorption spectra of selected vanadium compounds. *Physical Review B*, 30, 5596–5610.
- Wood, B., Wade, J., and Kilburn, M. (2008) Core formation and the oxidation state of the Earth: Additional constraints from Nb, V and Cr partitioning. *Geochimica et Cosmochimica Acta*, 72, 1415–1426.
- Woodland, A.B. and Koch, M. (2003) Variation in oxygen fugacity with depth in the upper mantle beneath the Kaapvaal craton, Southern Africa. *Earth and Planetary Science Letters*, 214, 295–310.
- Yurimoto, H. and Ohtani, E. (1992) Element partitioning between majorite and liquid: a SIMS study. *Geophysical Research Letters*, 19, 17–20.

MANUSCRIPT RECEIVED SEPTEMBER 13, 2010

MANUSCRIPT ACCEPTED APRIL 19, 2011

MANUSCRIPT HANDLED BY M. DARBY DYAR